AIAA 81-0333R

A Reattaching Free Shear Layer in Compressible Turbulent Flow

C. C. Horstman*
NASA Ames Research Center, Moffett Field, Calif.
and
G. S. Settles,† D. R. Williams,‡ and S. M. Bogdonoff§
Princeton University, Princeton, N. J.

A numerical simulation of the time-dependent, Reynolds-averaged, Navier-Stokes equations for the entire flowfield, employing a two-equation eddy viscosity turbulence model, is presented for free turbulent shear layer reattachment on inclined surfaces at high Mach number. The results are compared to the results of an investigation of a two-dimensional, free turbulent shear layer reattaching on an inclined surface at Mach 2.92 and at a high Reynolds number. The test geometry is specifically designed to isolate the reattachment process of a high-speed separated flow. Detailed comparisons of prediction and experiment are made in the free shear layer, at reattachment, and in the developing boundary layer downstream. These comparisons include mean surface quantities as well as mean and fluctuating flowfield quantities. Although the overall features of this complex flowfield are predicted, there are several deficiencies in the numerical solution, particularly in the region downstream of reattachment. Modifications of the turbulence model to correct these difficiencies are discussed.

Nomenclature

C_{f_∞}	= skin friction coefficient based on freestream conditions
k	= turbulent kinetic energy, $(\overline{u'^2}+\overline{v'^2}+\overline{w'^2})/2$
ℓ	= turbulent length scale, $\sqrt{k}/\omega$
M	= Mach number
p	= static pressure
P_k	= turbulence production term
R_t	= turbulence Reynolds number
u	= velocity in x or x' direction
v	= velocity in y direction
w	= velocity normal to u and v
x	= streamwise distance measured from separation corner (Fig. 1)
x'	= distance along ramp measured from leading edge (Fig. 1)
y	= distance normal to model surface: measured from plane of upstream flat plate in free shear layer, measured from model surface on ramp
$\beta,\beta^*,\gamma,\gamma^*$	= turbulent modeling constants
δ	= shear-layer or boundary-layer thickness
δ^*	= boundary-layer displacement thickness
θ	= boundary-layer momentum thickness
μ	= molecular viscosity
μ_t	= turbulent eddy viscosity
ρ	= density
τ	= shear stress
ω	= turbulent dissipation rate
$\langle(\,)\rangle$	= rms value

Subscripts

max	= maximum
w	= wall conditions
∞	= freestream conditions

Superscripts

$(\,)'$	= fluctuating quantity

Presented as Paper 81-0333 at the AIAA 19th Aerospace Sciences Meeting, St. Louis, Mo., Jan. 12-15, 1981, submitted March 9, 1981; revision received June 9, 1981. This paper is declared a work of the U.S. Government and therefore is in the public domain.

*Assistant Chief, Experimental Fluid Dynamics Branch. Associate Fellow AIAA.

†Professional Research Staff Member and Lecturer, Mechanical and Aerospace Engineering. Member AIAA.

‡Graduate Research Assistant.

§Professor and Chairman, Mechanical and Aerospace Engineering. Fellow AIAA.

Introduction

In the past several years, considerable advances have been made in the prediction of compressible viscous flowfields. For two-dimensional flows, with both adverse and favorable pressure gradients and even with small separated regions, various computational methods employing a two-equation eddy viscosity turbulence model do an adequate job of predicting the flowfields.[1,2] However, the computation of flowfields in which there are large separated zones has met with only limited success.[2-4] Large disagreements between numerical and experimental results are most prevalent in the reattachment region and downstream. Unfortunately, in these latter viscous compressible flow interactions, boundary-layer separation and subsequent reattachment are often intimately connected and it is difficult to scrutinize either phenomenon by itself.

A recent experimental investigation performed at Princeton University[5] has successfully isolated the reattachment process of a high-speed separated flow. This offers a unique opportunity to test the ability of a numerical technique and its associated turbulence model to correctly model the reattachment region and downstream boundary-layer redevelopment without the additional complication of modeling the separation process as well. In this study, an equilibrium turbulent boundary layer developed on a flat plate. The layer then separated at a sharp corner, forming a free shear layer that bridged a cavity to reattach upon an inclined ramp. The measurements included detailed mean surface and flowfield data as well as mass flow fluctuation data in the flowfield.

This paper presents a detailed comparison of numerical calculations and experimental results for the reattaching free shear layer described above. The calculations employed are solutions of the time-dependent, Reynolds-averaged Navier-Stokes equations, using a two-equation eddy viscosity turbulence model.[1] These comparisons test the ability to calculate not only the reattachment process and downstream boundary-layer growth, but also the development of the supersonic free shear layer. These three problems are, in a sense, separate and provide a severe test of the turbulence model and the computational techniques used. Based on these comparisons, deficiencies in the turbulence model are discussed and modifications to correct these deficiencies are proposed.

Description of Experiment

The experiment was conducted in the Princeton University 20×20 cm High Reynolds Number Supersonic Wind Tunnel at a freestream Mach number of 2.92 and a unit Reynolds

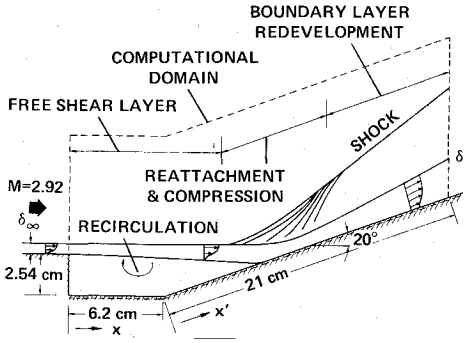

Fig. 1 Flow geometry and computational domain.

number of 6.7×10^7/m.[5] A sketch of the test model is shown in Fig. 1. A turbulent boundary layer developed initially on the flat plate (22.9 cm long), then separated over the sharp backward-facing step.The resulting free shear layer bridged a 2.54 cm deep cavity and reattached on a plane ramp inclined 20 deg to the horizontal. The movable ramp was adjusted so that there was essentially no change in pressure or flow direction when the boundary layer separated. (The average value of the ratio of plate pressure to cavity pressure over the test series was 1.04.) Two-dimensionality was verified with surface streak patterns and spanwise surface pressure and Preston tube measurements.

The measurements included surface pressure and skin friction, mean flowfield pressure and velocity distributions, and mass flow fluctuations throughout the flowfield. The skin friction data were obtained with Preston tubes and verified by combined wall wake law/velocity profile correlations. The mean velocity data were obtained from pitot and static pressure and total temperature measurements. Hot-wire anemometers were used to obtain the mass flow fluctuations. Further details of the experimental techniques, accuracy of the measurements, and results are contained in Ref. 5.

Solutions to the Navier-Stokes Equations

The partial differential equations used to describe the mean flowfield are the time-dependent, Reynolds-averaged Navier-Stokes equations for two-dimensional flow of a compressible fluid. Restrictions on the equations include the perfect gas assumption, constant specific heats, the Sutherland viscosity law, and zero bulk viscosity. The Wilcox-Rubesin[1] two-equation model was chosen for turbulence closure. The use of an algebraic eddy-viscosity turbulence model did not seem feasible for this complex flowfield. The problem is the a priori specification of a length scale everywhere in the flowfield. This would be especially difficult in the large recirculation zone and in the reattachment region where the length scale must make the transition from a free shear layer to an attached boundary layer. As a first effort to solve this flowfield, the use of the two-equation model, which calculates its own length scale, seemed appropriate.

For the Wilcox-Rubesin two-equation model, the flowfield equations are augmented by two additional partial differential equations: one for the turbulent kinetic energy k and another for the square of the dissipation rate ω^2.

$$\frac{\partial \rho k}{\partial t}+\frac{\partial}{\partial x}\left(\rho uk-\mu_k\frac{\partial k}{\partial x}\right)+\frac{\partial}{\partial y}\left(\rho vk-\mu_k\frac{\partial k}{\partial y}\right)=P_k-\beta^*\rho\omega k$$

$$\frac{\partial \rho\omega^2}{\partial t}+\frac{\partial}{\partial x}\left(\rho u\omega^2-\mu_{\omega^2}\frac{\partial \omega^2}{\partial x}\right)+\frac{\partial}{\partial y}\left(\rho v\omega^2-\mu_{\omega^2}\frac{\partial \omega^2}{\partial x}\right)$$

$$=\gamma\frac{\omega^2}{k}P_k-\left\{\beta+\left[\left(\frac{\partial \ell}{\partial x}\right)^2+\left(\frac{\partial \ell}{\partial y}\right)^2\right]\right\}\rho\omega^3$$

where P_k is the production term for the kinetic energy of turbulence (given in Refs. 1 and 2) and the diffusivities μ_k and $\mu_{\omega^2}=\mu+0.5\mu_t$. β^*,β, and γ are modeling constants.

The Wilcox-Rubesin model uses the eddy-viscosity hypothesis; that is, the Reynolds stress, turbulent heat flux, and kinetic energy flux terms are assumed to be related to the mean flow velocity, temperature, and kinetic energy gradients through an eddy transport coefficient that is simply added to the corresponding molecular viscosity or transport coefficient. The turbulent eddy viscosity μ_t is expressed in terms of k and ω:

$$\mu_t=\gamma^*\rho(k/\omega)$$

where γ^* is an exponential damping term that depends on a turbulent Reynolds number, $R_t=\rho\sqrt{k}\ell/\mu$. This Reynolds number is based on a length scale of the turbulence ℓ, defined as $\ell=\sqrt{k}/\omega$. The complete equations, including the equations and constants for the turbulence model, are described in Ref. 2. This model differs from most other eddy-viscosity models in that the constitutive relation between the Reynolds stress tensor and the mean flow properties has been modified to represent anisotropic normal Reynolds stress phenomena. The stress tensors for this model are given in Refs. 1 and 2.

Numerical Method

The numerical procedure used here is the basic explicit second-order, predictor-corrector, finite-difference, time-splitting method of MacCormack,[6] modified by the efficient explicit-implicit characteristic algorithm of Ref. 7. A description of this method, along with its adaptation to multiequation turbulence models, is contained in Refs. 2 and 8.

Computational Domain

The computational domain is shown in Fig. 1. The upstream boundary was placed at the separation corner to avoid possible difficulties there. A mesh was developed that allowed a variable point spacing in each coordinate direction. One set of grid lines was placed normal to the freestream direction and the other parallel to the model surface. The total mesh size was 90 points in the streamwise direction and 82 points normal to the model surface. In the streamwise direction mesh spacing varied from 0.065 cm near the corner to 0.50 cm near the downstream boundary. In the direction normal to the surface an exponentially stretched spacing was used near the wall followed by a uniform spacing. The distance of the first y mesh point from the model wall was selected small enough so that the solutions are independent of spacing (typically within $y^+\min\equiv y\sqrt{\tau_w\rho_w}/\mu_w<0.5$).

Boundary Conditions

The boundaries of the computational mesh extended in the vertical direction from the model surface to the freestream and in the flow direction from $x=0$ to $x'=21$ cm. The upstream boundary conditions were prescribed by a combination of uniform freestream conditions and the result of a boundary-layer computation[1] along the flat-plate surface. The boundary-layer program was run for a distance that insured a match of the experimental and numerical boundary-layer displacement thicknesses at $x=-2.54$ cm. At the vertical wall below the corner, the pressure was set equal to the freestream pressure (to match the experimental results), and the temperature was set equal to the model wall temperature. The vertical velocity was set equal to zero and the horizontal velocity was set equal to $0.0005\ u_\infty$. (When an inflow velocity of zero was used a solution could not be obtained.) The downstream boundary was positioned far enough aft so that all of the gradients in the flow direction could be set to zero. This boundary condition was verified by the lack of any substantial change in the numerical results when the location of the downstream boundary was changed.

At the model surface, no-slip boundary conditions are applied along with a constant wall temperature and the turbulent kinetic energy set equal to zero. Near the surface, where the dissipation of ω^2 is approximately equal to its molecular diffusion, the following analytical solution can be developed:

$$\omega = 20\mu/\beta\rho y^2$$

This equation was found to be valid in equilibrium boundary layers for $y^+ \equiv y\sqrt{\tau_w \rho_w}/\mu_w \leq 10$. This expression was used in the present computation as follows: The dissipation rate equation was solved numerically for $y^+ \geq 4$ and patched smoothly to this expression (used as a boundary condition) for smaller values of y^+. (This procedure was also used by Wilcox and Rubesin in their boundary-layer solutions.[1])

In the freestream and along the upper boundary, a minimum value of ω^2 was prescribed to prevent the turbulence length scale from growing too large. The maximum value of the length scale used for the present computations ($\ell_{max} = 0.2\delta$) was four times the value used as the outer edge boundary condition in the boundary-layer code described in Ref. 1. At convergence this limit did not influence the present results. The freestream and upper boundary disturbance level was set at $\sqrt{k}/u_\infty = 0.006$, which amounts to $\langle(\rho u)'\rangle/\rho_\infty u_\infty = 0.025$.

Numerical Accuracy

The procedure employed is second-order accurate in space and mixed between first- and second-order accurate in time. In the vicinity of shock waves a fourth-order smoothing term is used. To check the accuracy of the present computer code a detailed comparison was made with the computed results of a fourth-order accurate boundary-layer code.[1] Comparisons were made for several Mach numbers with both zero and adverse pressure gradients. In all cases the results from the two computer codes agreed to within 10%. These included both the mean and turbulent flowfield variables. As an additional check on the accuracy of the present solution, a second solution was obtained employing a more coarse grid (60×50). These results were at most 5% different from those employing the finer grid. Several other grid refinement studies have been made using the present computer code and turbulence model for other flow geometries.[2,9] Provided the streamwise spacing is less than 0.5δ near the interaction region and at least 25 mesh points are used across the viscous layer, further grid refinements have a negligible effect on the results. For the present study a spacing of 0.2δ was used near reattachment and 40 mesh points were used across the viscous layer.

Results and Discussion

A map of the computed Mach contour lines in the flowfield is shown in Fig. 2. In agreement with the experimental results, the incoming turbulent boundary layer separates at the corner without turning, forming a free shear layer. This layer spreads more rapidly into the cavity than into the outer, supersonic flow, and reattaches on the ramp at a point slightly below the geometric extension of the flat plate onto the ramp surface. The average computed pressure on the cavity floor was $0.97p_\infty$, which agrees exactly with the experiment. Downstream of reattachment a new boundary layer develops on the ramp. Detailed comparisons with the experimental data are presented in two parts: the free-shear-layer results and the reattachment and downstream boundary-layer results.

Free Shear Layer

The computed and experimental velocity profiles are compared at several streamwise locations in the free shear layer in Fig. 3. Also shown is a comparison of computed and experimental boundary-layer profiles upstream of the separation point on the flat plate ($x = -2.54$ cm). These upstream results were computed using the boundary-layer code mentioned earlier. In the shear layer the computed

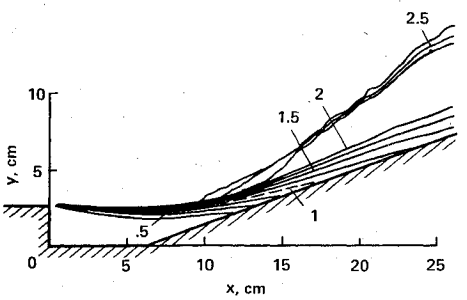

Fig. 2 Computed contour plot of Mach number.

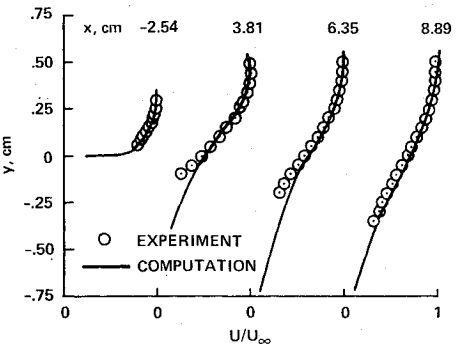

Fig. 3 Comparison of computations and velocity profile measurements in the free shear layer.

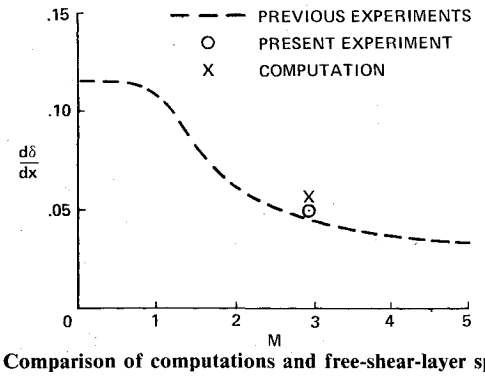

Fig. 4 Comparison of computations and free-shear-layer spreading rate measurements.

results are in good agreement with the experiment for velocity ratios greater than 0.5. However, for the lower velocity ratios the computed results are substantially greater than the data. This indicated that the computed shear layer spread into the cavity farther than the measured one, resulting in a larger shear-layer thickness before reattachment. At the lower values of velocity the viscous terms in the momentum equation become relatively more important, so any lack of validity in the turbulence model equations is expected to cause larger differences between the computations and measurements in this region. Apparently the turbulence model produces too much diffusion here. At the last station compared ($x = 8.89$ cm), the results show better agreement than for the previous stations. The maximum computed reverse velocity in the cavity is $0.17u_\infty$; however, experimental data were not obtained in this region and no comparison is possible.

The free-shear-layer spreading rates for both the experimental and the computed results have been calculated by defining the shear-layer thickness δ as the distance between $(u/u_\infty)^2 = 0.1$ and 0.9.[10] The spreading rate was evaluated after velocity profile similarity developed in the shear layer, which required a distance downstream of separation of 18 initial boundary-layer thicknesses in the experiment and 22 thicknesses in the computation. A comparison is shown in Fig. 4 along with a line representing average values from

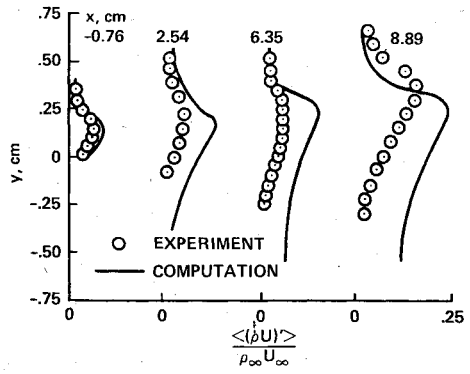

Fig. 5 Comparison of computations and rms mass flow fluctuation profile measurements in the free shear layer.

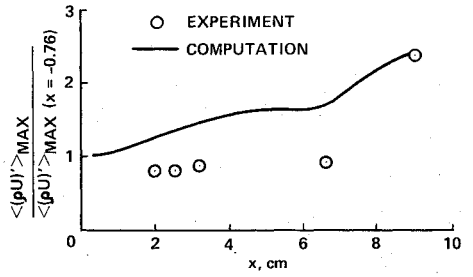

Fig. 6 Comparison of computations and maximum rms mass flow fluctuation measurements in the free shear layer.

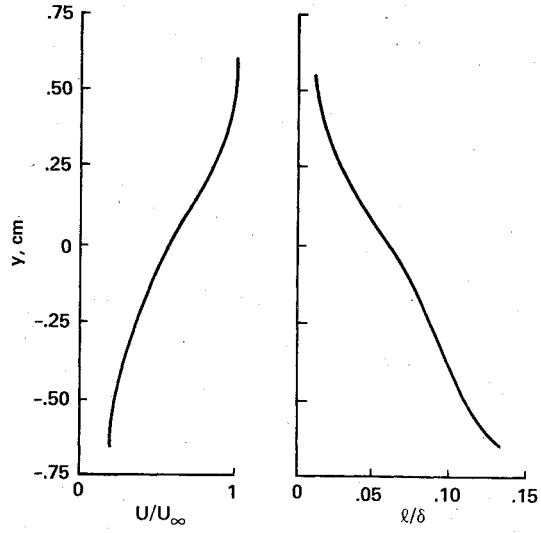

Fig. 7 Computed velocity and length scale profile in the free shear layer, $x = 6.35$ cm.

previous high Reynolds number, compressible, free-shear-layer experiments.[11] Although the computed profile shapes were not in good agreement with experiment, the growth rate of the width of the profile is in good agreement.

The present computations provide a significant improvement over previous computational results,[11] which predicted the incompressible value of the spreading rate ($d\delta/dx = 0.12$) at supersonic Mach numbers. More recent computations by Saffman[12] and by Oh and Bushnell[13] also predict the correct compressible spreading rates. Saffman's turbulence model is an earlier version of the one used in the present computations; in the model used by Oh and Bushnell an additional term modeled the pressure-velocity correlation, which was a function of Mach number. The present calculations require no additional terms for compressible flow. It is significant that the present computational framework has captured the physics of this compressible spreading phenomenon, even though the phenomenon is known to violate Morkovin's hypothesis.[14]

The computed and experimental rms mass flow fluctuations are compared at several streamwise locations in the free shear layer in Fig. 5. Also shown is a comparison upstream of the separation point on the flat plate ($x = -0.76$ cm). To compare the computed and measured turbulent fluctuations, several assumptions were made. The mass flow fluctuations were measured experimentally, and the total turbulent kinetic energy was computed and converted to rms mass flow fluctuations, $\langle(\rho u)'\rangle$. This latter computation was carried out as follows. It was assumed that the ratio of the streamwise to lateral to normal velocity fluctuations was 4/3/2, and that the total temperature and pressure fluctuations were negligible compared with the streamwise velocity fluctuations. Thus the mass flow fluctuations become a function of the computed turbulent kinetic energy, local Mach number, and density.[15] For adiabatic flows away from shock waves these assumptions are reasonable[15] and should provide at least a qualitative comparison of the experimental and computed results. But the validity of these assumptions is unknown within the shock/boundary-layer interaction.

In general the measured mass flow fluctuation values are overpredicted throughout the flowfield. In the lower part of the shear layer the data are overpredicted by a factor of 10. This large overprediction in the cavity is the result of too much diffusion in the turbulence model equations at low velocities, which leads to incorrect mean velocity profiles, as shown in Fig. 3. At the last station ($x = 8.89$ cm) the computed and experimental results are at least qualitatively similar, although the levels disagree.

To examine the rate of growth of the fluctuation levels, both the measured and computed peak values have been normalized by their upstream values and plotted in Fig. 6. This comparison shows that the measured normalized peak values do not increase in magnitude until far downstream where velocity profile similarity is reached ($x \sim 6$ cm). The computed normalized peak values increase gradually until similarity is reached ($x \sim 7$ cm) and then increase more rapidly downstream. The agreement between the computed and measured values at the downstream location could be fortuitous.

Since the mass flow fluctuations were grossly overpredicted in the lower part of the shear layer, it may be instructive to examine the computed turbulent length scale distribution through the shear layer. The computed values of the mean velocity ratio and of the turbulent length scale, normalized by the shear-layer thickness, are shown in Fig. 7 for $x = 6.35$ cm. The results show that the length scale increases continuously as y and the velocity ratio decrease. It is believed that this behavior is incorrect, and that the length scale should reach a maximum in the shear layer and then decrease as y decreases. However, there are no measurements available to support this speculation. If so, then any turbulence model improvements should be directed toward the length scale or the dissipation equation.

Reattachment and Boundary-Layer Redevelopment

Comparisons of the computed and experimental surface pressure and skin friction distributions on the ramp are shown in Fig. 8. There is general qualitative agreement between the computed and measured values but several important differences are also noted. First, the computed reattachment point is at 5.2 cm and the experimental reattachment point is at 6.76 cm. This difference is a result of the computed shear layer extending too far into the cavity, thus reattaching to the ramp surface too far upstream. This also explains the differences between the predicted and measured pressure distributions. The predicted pressure first increases upstream of the experimental pressure increase, and requires about a 12% greater distance to reach its final value. Since the

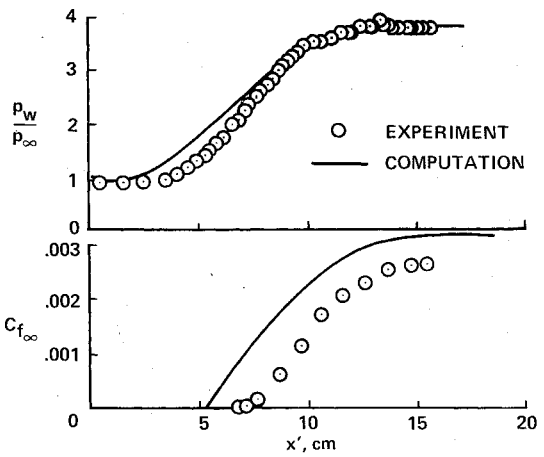

Fig. 8 Comparison of computations and measured surface pressure and skin friction on the reattachment ramp.

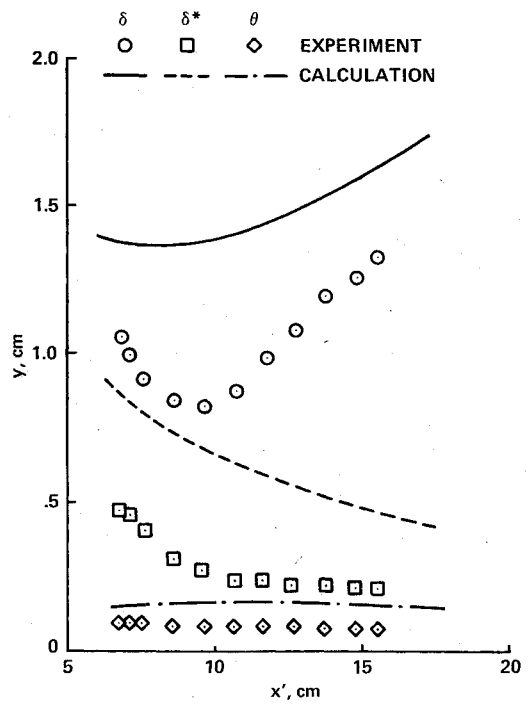

Fig. 9 Comparison of computations and measured boundary-layer thicknesses on the reattachment ramp.

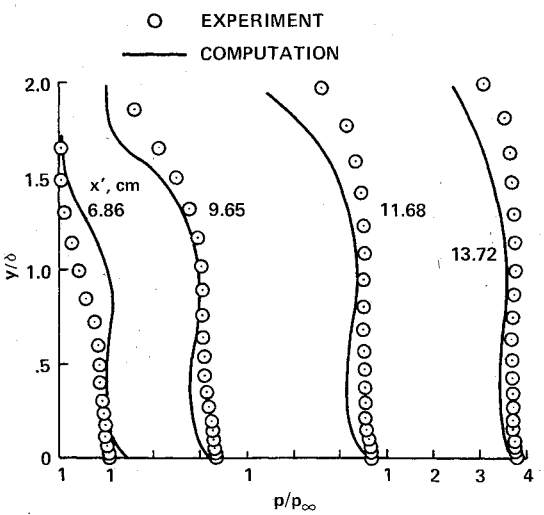

Fig. 10 Comparison of computations and static pressure profile measurements downstream of reattachment.

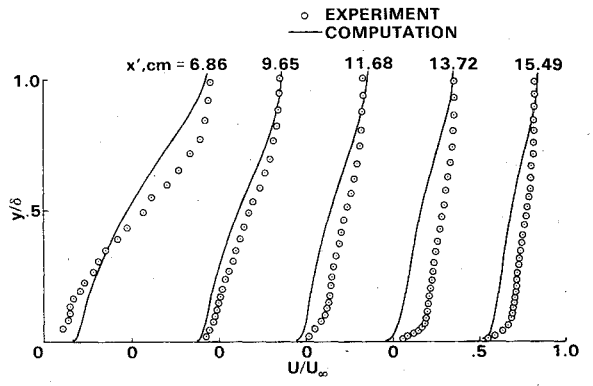

Fig. 11 Comparison of computations and velocity profile measurements downstream of reattachment.

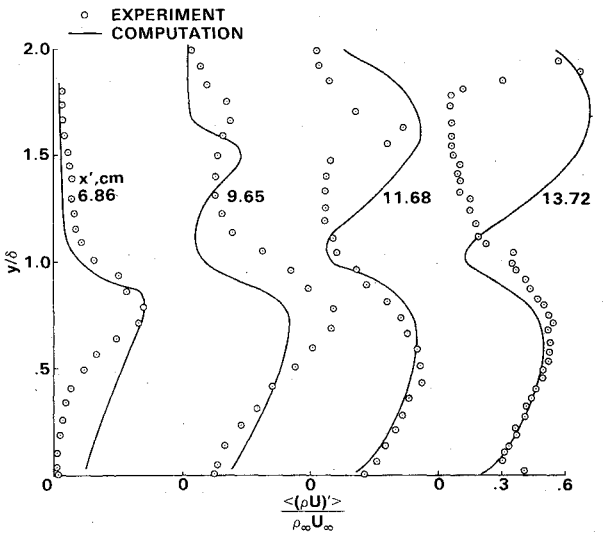

Fig. 12 Comparison of computations and rms mass flow fluctuation profile measurements downstream of reattachment.

computed shear-layer thickness was also about 12% larger than the experimental value, these results are reasonable and in agreement with the free interaction theory discussed in Ref. 5. At the downstream end of the interaction the pressure is correctly predicted, but the skin friction is overpredicted by 20%.

Figure 9 compares the computed and experimental development of the boundary-layer thickness, displacement thickness, and momentum thickness downstream of reattachment. Although the correct trends of all three thicknesses are predicted, the values are too large. The boundary-layer thickness is overpredicted by as much as 60%. This is because the incoming shear layer is thicker than the experimental shear layer and because the large overprediction of turbulent kinetic energy and length scale in the lower portion of the incoming shear layer also tends to thicken the boundary-layer at reattachment. To allow a comparison of computed and experimental flow development downstream of reattachment despite this difference in thickness, the distances from the wall have been normalized by the local boundary-layer thickness in the remaining figures.

The computed and experimental static pressure profiles are compared at several streamwise locations in Fig. 10. The first station is located at the experimental reattachment point. In the boundary layer ($y/\delta < 1$), the predicted distributions show a larger variation normal to the surface than do the measured values. However, if the pressure increase due to turbulent kinetic energy ($2/3\rho k$) were added to the computed static pressure, the agreement with the experiment would improve. This correction is up to 15% for the present flowfield. This was not done because the experimental results were obtained

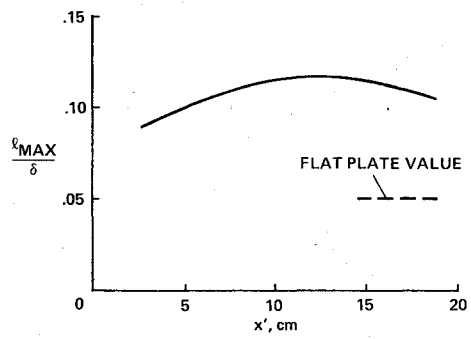

Fig. 13 Computed variation of maximum length scale downstream of reattachment.

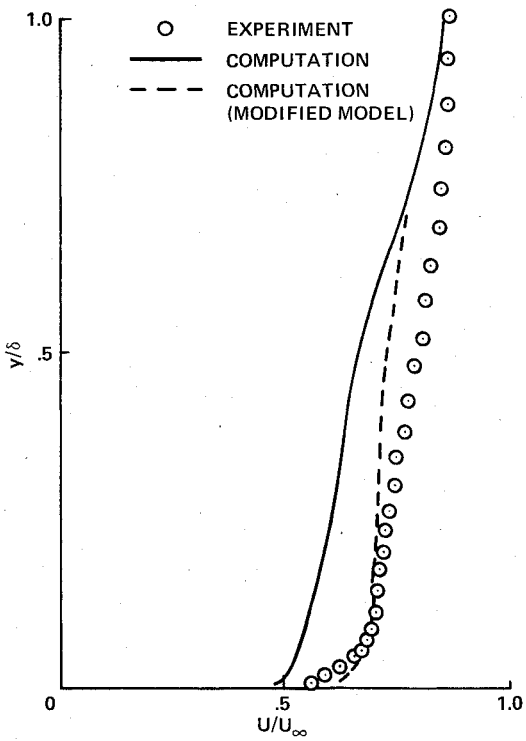

Fig. 14 Comparison of computations with the original and modified turbulence models and velocity profile measurements, $x' = 13.72$ cm.

with a static pressure probe that is probably insensitive to this increased kinetic pressure. In the outer portion of the flow the calculated results show the correct trends, and differences between the computation and the experiment can be attributed to the choice of δ as a scaling parameter outside the boundary layer.

Figure 11 compares the computed and experimental mean velocity profiles at reattachment and downstream. The computed and measured profiles have similar shapes, but the computation fails to predict the correct development downstream. The fact that the computed profiles fail to fill out as fast as the measured profiles has also been shown for other experimental test cases downstream of reattachment.[2,4,9] This deficiency will be discussed in greater detail later. The disagreement between the two profiles at reattachment ($x = 6.86$ cm) is due in part to the fact that the computed solution reattached earlier (at 5.2 cm).

The computed and measured values of the rms mass flow fluctuations at reattachment and downstream are compared in Fig. 12. Considering the assumptions made to convert the computed kinetic energy to mass flow fluctuations, the agreement is reasonably good. In the boundary layer the two downstream profiles are well predicted. The profile at reattachment shows the same differences as in the shear layer (Fig. 5). Outside the boundary layer, both the computations and the experiment show the same magnitude of increased fluctuations due to the flow through the recompression shock wave (located near $y/\delta = 1.8$ for the last three stations). However, the vertical extent of this increase is overpredicted. The thickness of the computed recompression shock wave determined from the mean flow quantities was less than 0.15 δ (see Fig. 2). At $x = 13.72$ cm the 60% mass flow fluctuation level outside the boundary layer is calculated from a 12% turbulent kinetic energy level.

At $x = 11.68$ and 13.72 cm the velocity profiles are poorly predicted, but the fluctuation levels are well predicted. Therefore the computed length scale must be in error. Experimental evidence from spark shadowgrams suggests that this portion of the flowfield is dominated by large eddies,[5] which in turn suggests a large increase in turbulence length scale not accounted for in the computed solution.

The computed values of the maximum length scale in the boundary layer, normalized by the local boundary-layer thickness, are shown in Fig. 13. Also shown is the flat-plate value for an equilibrium turbulent boundary layer. These results show a significant increase over the flat-plate value in the reattachment region and downstream, but the previous comparisons with the experiment suggest that this is not enough. To test this hypothesis, the flowfield was recomputed while the length scale was increased arbitrarily by a factor of three in the middle portion of the boundary layer downstream of reattachment. This resulted in two changes in the computed results: 1) the boundary-layer thickness increased slightly, and 2) the mean velocity profiles changed significantly. A typical profile at $x = 13.72$ cm is shown in Fig. 14. The recomputed velocity distribution with the larger length scale is in much better agreement with the experiment. The kinetic energy distribution remained the same, as is shown in Fig. 12, and the surface skin friction increased 20%.

These results demonstrate the need for an improved length scale prediction in the turbulence model equations. Perhaps the best way to approach this problem is to perform a sensitivity analysis, following Dwyer,[16] to find out which terms or constants in the length scale or dissipation equation need to be modified for improved predictions. This is a formidable task and remains a subject for later study. Also, additional experiments are planned by the Princeton authors of this paper to obtain more direct measurements of the turbulent length scales. It is also questionable whether an eddy-viscosity turbulence model can adequately model the physics of the reattachment region where a highly nonequilibrium flow situation occurs. Clearly the turbulence structure is out of equilibrium with the mean flow. A more appropriate turbulence model for this region may be the algebraic Reynolds stress model or other higher-order models. Work at Ames is proceeding in this direction and preliminary results have shown improvements when an algebraic Reynolds stress model is used.

Conclusions

A detailed experimental documentation of the mean and fluctuating flow throughout a reattaching free shear layer in compressible turbulent flow has been made. These data have been used to assess the validity of corresponding numerical computations and to guide turbulence modeling changes. Numerical solutions of the time-dependent, Reynolds-averaged Navier-Stokes equations employing a two-equation turbulence model have been compared with the experimental results. In general, the overall features of this complex flowfield have been predicted, although there are several areas of the flowfield in which significant improvements in the turbulence modeling are required if good agreement with experiment is to be achieved.

For the free shear layer the numerical results adequately predict the total spreading rate, which is a significant achievement by itself. Also, good agreement was obtained

with the detailed velocity profiles in the high-momentum portion of the layer. However, poor agreement was obtained in the low-momentum half of the shear layer, where the mean velocity and the turbulent kinetic energy were overpredicted. This suggests that the turbulence model is producing too much diffusion and that the turbulent length scale is too large in this region.

Because the initial spreading of the computed shear layer into the cavity was too rapid, the computed reattachment point was upstream of the experimental point; as a result, the boundary layer was too thick. Downstream of reattachment, good agreement was obtained with the turbulent mass flow fluctuations, but the predicted mean velocity profiles failed to develop as rapidly as the experimental ones. This suggested that the computed length scale was underpredicted in this region. An increased length scale was employed in a second computation and improved agreement with the experiment was obtained.

Although the present investigation has not provided an improved turbulence model, it has isolated the area where improvements are needed, namely the second turbulence model equation for the dissipation rate, which determines the length scale. Before such improvements can be made, a sensitivity analysis must be performed. In the flow studied here we have found two major areas of disagreement; in one the length scale should be decreased and in the other it should be increased. Thus, although the need for turbulence model improvements is clear, it is significant that at least some features of the experimental flowfield were predicted adequately.

References

[1] Wilcox, D. C. and Rubesin, M. W., "Progress in Turbulence Modeling for Complex Flow Fields, Including Effects of Compressibility," NASA TP-1517, April 1980.

[2] Viegas, J. R. and Horstman, C. C., "Comparison of Multiequation Turbulence Models for Several Shock Boundary-Layer Interaction Flows," *AIAA Journal,* Vol. 17, Aug. 1979, pp. 811-820.

[3] Seegmiller, H. L., Marvin, J. G., and Levy, L. L. Jr., "Steady and Unsteady Transonic Flow," *AIAA Journal,* Vol, 16, Dec. 1978, pp. 1262-1270.

[4] Settles, G. S., Fitzpatrick, T. J., and Bogdonoff, S. M., "Detailed Study of Attached and Separated Compression Corner Flowfields in High Reynolds Number Supersonic Flow," *AIAA Journal,* Vol. 17, June 1979, pp. 579-585.

[5] Settles, G. S., Baca, B. K., Williams, D. R., and Bogdonoff, S. M., "A Study of Reattachment of a Free Shear Layer in Compressible Turbulent Flow," AIAA Paper 80-1408, July 1980 (submitted to *AIAA Journal*).

[6] MacCormack, R. W., "Numerical Solution of the Interaction of a Shock Wave With a Laminar Boundary Layer," *Lecture Notes in Physics,* Vol. 8, Springer-Verlag, New York, 1971, pp. 151-163.

[7] MacCormack, R. W., "An Efficient Numerical Method for Solving the Time-Dependent Compressible Navier-Stokes Equations at High Reynolds Number," *Computing in Applied Mechanics,* AMD Vol. 18, American Society of Mechanical Engineers, New York, 1976.

[8] Coakley, T. J. and Viegas, J. R., "Turbulence Modeling of Shock Separated Boundary-Layer Flows," Paper presented at the Symposium on Turbulent Shear Flows, University Park, Pa., April 1977.

[9] Johnson, D. A. and Horstman, C. C., "A Comprehensive Comparison Between Experiment and Prediction for a Transonic Turbulent Flow," AIAA Paper 80-1407, Snowmass, Colo., July 1980 (submitted to *AIAA Journal*).

[10] Schlichting, H., *Boundary Layer Theory,* McGraw-Hill Book Co., New York, 1955.

[11] Birch, S. F. and Eggers, J. M. "A Critical Review of the Experimental Data for Developed Free Turbulent Shear Layers," NASA SP-321, July 1972, Paper 2.

[12] Saffman, P. G., "Development of a Complete Model for the Calculation of Turbulent Shear Flows," Paper presented at the 1976 Duke Turbulence Conference, Durham, N. C., April 1976.

[13] Oh, Y. H. and Bushnell, D. M., "Influence of External Disturbances and Compressibility on Free Turbulent Mixing," NASA SP-347, March 1975, Paper 10.

[14] Bradshaw, P., "Compressible Turbulent Shear Layers," *Annual Review of Fluid Mechanics,* Vol. 9, 1977, pp. 33-54.

[15] Horstman, C. C. and Rose, W. C., "Hot-Wire Anemometry in Transonic Flow," *AIAA Journal,* Vol. 15, March 1977, pp. 395-401.

[16] Dwyer, H. A., "A Study of Turbulent Flow with Sensitivity Analysis," AIAA Paper 80-1397, July 1980.